Radiation Physics and Chemistry 223 (2024) 111899

Contents lists available at ScienceDirect

Radiation Physics and Chemistry

journal homepage: www.elsevier.com/locate/radphyschem

Detector-specific separation of spectral components from repetitive measurements in environmental radiation monitoring

Ignasi Reichardt *, Agustín Cerezo, Elena Prieto, Marçal Salvadó

Unitat de Física Mèdica, Universitat Rovira i Virgili, Facultat de Medicina i Ciències de la Salut. C/Sant Llorenç 21, Reus, E43201, Catalonia, Spain

ARTICLE INFO

Keywords:
Gamma-ray spectrometry
Environmental radioactivity monitoring
Naturally occurring radionuclides
Full spectrum analysis

ABSTRACT

Gamma-ray spectrometers for environmental radiation monitoring on field routinely record short-duration spectra. Under normal conditions, these spectra are the sum of a constant background plus photo-peaks from natural emitters, and their resulting bremsstrahlung and Compton scattering radiation. For each monitor, the constant background is specific to the monitor components and the composition of the soil and of the surroundings. On the other hand, the spectrum of the natural gamma-ray emitters also depends on the aspects above, but may also have variable intensity owing to aerosol scavenging in case of rain.

We present a case of a large network of detectors where it is unpractical to perform dedicated simulations or measurements of calibration sources. To overcome this difficulty, we propose a method to remotely and systematically extract fundamental spectra. For each spectrum we measure the activity concentration of natural emitters. Then, for each channel, the activity concentration of each natural emitter constitute the coefficients of an equation, where the unknowns are the fundamental spectra of the natural emitters and of the constant background. After repeated measurements, we can construct an over-determined system of equations that is solvable as a non-negative least-squares problem. As a result of the least-squares minimization we obtain the separate spectra of the constant background and of the most relevant natural gamma-ray emitters.

This method allows to produce highly specific fundamental spectra for each monitor. This improves the characterization of each monitor and allows to accurately reconstruct subsequently measured spectra using the Full Spectrum Analysis.

1. Introduction

The Spanish Nuclear Safety council requires to be informed about any release of radioactive substances resulting on a dose for the population of 1 μSv per hour or 8 mSv per year (CSN, 2023). The exact same requirements apply in other countries like Brazil, Argentina or Uruguay and the United States of America (USNRC, 2021). The regulatory requirements refer to the dose from isotopes resulting from human activities, not to natural radioactivity. Therefore, it is crucial that detection networks are capable to tell apart the origin of the received dose.

For the sake of broad spatial coverage with robust detectors and the possibility to use built-in software, most countries construct networks of gamma dose meters to measure gamma-emitting gasses or aerosols (Abida et al., 2008; Hiemstra et al., 2009; Neumaier et al., 2016; Stöhlker et al., 2018; Ángeles Ontalba et al., 2022). However, it is also possible to perform near-real-time monitoring with gamma-ray spectrometry, which in addition provides pollutant identification and false-positive suppression (Toivonen et al., 2008; Baeza et al., 2017; Cerezo et al., 2024). If only the gamma dose is desired, then it is possible to reduce the spectral information into the ambient dose equivalent, H*(10) (Casanovas et al., 2016).

The full exploitation of spectral data demands the application of the so-called Full Spectrum Analysis (FSA). This is usually done by constructing fundamental spectra either by Monte-Carlo simulations (Androulakaki et al., 2016) of by measurement of calibration spectra that are enriched in one isotope at a time (Caciolli et al., 2012). Then, every new spectrum is reconstructed as a linear combination of the fundamental spectra, where the proportionality factors are the activity concentrations of the isotopes of interest in a new measurement. Here we attempt to solve the inverse problem, and use the activity concentrations to find the fundamental spectra.

In Catalonia, North-Eastern Spain, our group analyzes the data from 35 gamma-ray spectrometers. These belong to the Environmental Radioactivity Surveillance Network of Catalonia (XVRAC)[1] of the Generalitat de Catalunya (Catalan government). The XVRAC monitors are

* Corresponding author.
E-mail address: ignasi.reichardt@urv.cat (I. Reichardt).

[1] http://xvrac.fmurv.cat.

https://doi.org/10.1016/j.radphyschem.2024.111899
Received 26 February 2024; Received in revised form 28 May 2024; Accepted 2 June 2024
Available online 4 June 2024

concentrated in the South, near the Ascó and Vandellòs nuclear power plants. However we also have monitors along the French border and in other towns, with sparser coverage of the whole region. We are also in charge of similar equipment in other countries (Argentina, Uruguay, Paraguay and Mexico). The first monitors were installed in 2006, and the network has been progressively expanded since then. During this time, the available technology and funding have determined the components in use in each monitoring station. The early types were mostly $2'' \times 2''$ NaI(Tl) crystals; later, several $2'' \times 2''$ $LaBr_3$(Ce) were installed (Casanovas et al., 2012a); and more recently we are opting for the $2'' \times 2''$ SrI_2(Eu) crystals (Cerezo et al., 2023). The varying locations of the monitors makes the soil, the architecture of the monitoring station, and other details (most notably, the use of a particulate filter (Casanovas et al., 2014)), difficult to model in general Monte-Carlo simulations. Therefore, we need to develop remote calibration and characterization methods.

Each monitor records a gamma-ray spectrum every ten minutes. The Catalan network and the ones in Argentina, Uruguay, Paraguay and Mexico generate a combined 1.5 million spectra every year that are available for us to analyze. With such data volume, we are focused on the development of automated analysis for near real-time monitoring and early warning (Cerezo et al., 2023). In a typical spectrum we record the photo-peaks of the ^{220}Rn descendants (^{212}Pb and ^{208}Tl), and those from the ^{222}Rn descendants (^{214}Pb and ^{214}Bi). Among other natural gamma-ray emitters (e.g.^{40}K, $e^+ + e^-$, ^{228}Ac), the above-mentioned isotopes are of particular interest for this work because their intensity depends on the weather conditions, mainly on rain (Fujinami, 1996; Paatero and Hatakka, 1999).

In this article we present a method to remotely extract fundamental spectra of prominent naturally-occurring radioisotopes. For this goal we use a linear algorithm fed with several thousand spectra. As a result we obtain spectral components that contain the constant background on one hand, and each of the natural varying gamma-emitters on the other. This ought take into account that for each component there is an associated Compton scattering and bremsstrahlung radiation specific to each monitor due to the varying characteristics of the surroundings and of the equipment. In a future step we can use each fundamental spectrum that appears recurrently to identify anomalies produced by isotopes of artificial origin in a framework of full spectrum analysis.

2. Methods

First and foremost, we need the spectra to be stable against peak shifts resulting from temperature-dependence of the channel-energy correspondence. For this we apply the method from Casanovas et al. (2012b).

Once the spectra are stabilized, we compute the count rates of the ^{212}Pb (238.6 keV), ^{214}Pb (351.9 keV), ^{208}Tl (583.2 keV), and ^{214}Bi (609.3 keV) photo-peaks. Within the energy resolution of our detectors, the ^{212}Pb and ^{214}Pb peaks overlap, as well as the ^{208}Tl and ^{214}Bi peaks. To estimate their count rate we developed an automated procedure of Gaussian fitting, where the two peaks are fitted together with a straight continuum. For this we consider a spectral window that goes from the energy of the lowest energy peak minus 3σ, to the energy of the highest energy peak plus 3σ (with σ being the energy resolution at the energy of each peak). The count rates are then divided by the simulated detector efficiency from Casanovas et al. (2012a) and Cerezo et al. (2023), and also by the peak probability, hence resulting in measurements of activity concentration. In fact, these quantities only need to be proportional to the activity concentration, so this last step is not strictly necessary. Nevertheless, the four activity concentrations are measured from every spectrum, i.e., every ten minutes, which results in about 4320 measurements over the course of a month (Fig. 1). We choose data from the month of May 2023 for four field monitors from the Catalan network with different locations and characteristics. The fact of having a few rain episodes in the data favors the variability of the ^{222}Rn descendants, which is convenient for the subsequent analysis. In addition to the field data we used the data set from Cerezo et al. (2023), recorded using two reference monitors in our lab (Table 1).

Table 1
Monitors selected in this work to be representative of different locations, crystal sizes and crystal compositions. The monitor at Roses measures on a particulate filter that is exchanged every five days, and has a pump that forces an air flow of 10 m^3/h. The rest of monitors measure directly.

ID	Location	Crystal	Filter
9	Roses	$2'' \times 2''$ $LaBr_3$(Ce)	Yes
18	Sant Jaume d'Enveja	$1'' \times 1''$ $LaBr_3$(Ce)	No
31	Torre de l'Espanyol	$2'' \times 2''$ $LaBr_3$(Ce)	No
33	Pratdip	$2'' \times 2''$ SrI_2(Eu)	No
80	Lab	$2'' \times 2''$ $LaBr_3$(Ce)	No
90	Lab	$2'' \times 2''$ SrI_2(Eu)	No

Our key assumption to find the spectral components is that for each spectrum, the i^{th} energy bin has a count rate s_i consisting of a constant background $x_{0,i}$ plus a contribution from each of the natural gamma-emitters mentioned above. This assumption is equivalent to what we used in our previous work (Cerezo et al., 2023) to clean the influence of the main natural photo-peaks from spectral Regions of Interest (ROIs) under monitoring. In Cerezo et al. (2023) the ROIs of ^{131}I, ^{137}Cs and ^{60}Co were defined as the spectral band comprising 2σ about the central energy of each photo-peak. Here, instead of using ROIs, we use the proportional cleaning method for each spectral channel separately.

Each contribution to a spectral channel consists of the (unknown) fundamental spectrum multiplied by the intensity of the corresponding photo-peak. The proportionality factors are the activity concentrations mentioned above, which we note by $I_{^{214}\text{Pb}}$, $I_{^{214}\text{Bi}}$, $I_{^{212}\text{Pb}}$, and $I_{^{208}\text{Tl}}$. Then:

$$s_i = x_{0,i} + I_{^{214}\text{Pb}} x_{1,i} + I_{^{214}\text{Bi}} x_{2,i} + I_{^{208}\text{Tl}} x_{3,i} + I_{^{212}\text{Pb}} x_{4,i} \tag{1}$$

The unknowns x_0, x_1, x_2, x_3, x_4 are the fundamental spectra of the constant background and of the component varying with ^{214}Pb, ^{214}Bi, ^{208}Tl, and ^{212}Pb respectively, and encode a spectral shape that can be upscaled or downscaled according to the peak intensities. After many measurements we can construct an over-determined system of N equations, where $N \sim 4320$ in the monthly data sets mentioned above:

$$\begin{cases} s_i^{(1)} = x_{0,i} + I_{^{214}\text{Pb}}^{(1)} x_{1,i} + I_{^{214}\text{Bi}}^{(1)} x_{2,i} + I_{^{208}\text{Tl}}^{(1)} x_{3,i} + I_{^{212}\text{Pb}}^{(1)} x_{4,i} \\ \dots \\ s_i^{(N)} = x_{0,i} + I_{^{214}\text{Pb}}^{(N)} x_{1,i} + I_{^{214}\text{Bi}}^{(N)} x_{2,i} + I_{^{208}\text{Tl}}^{(N)} x_{3,i} + I_{^{212}\text{Pb}}^{(N)} x_{4,i} \end{cases} \tag{2}$$

This system is solvable as a non-negative least-squares problem, that is finding the positive values of x that minimize the norm of the vector $A\vec{x}_i - \vec{s}_i$:

$$\min_{x_i \geq 0 \forall i} \|A\vec{x}_i - \vec{s}_i\|^2 \tag{3}$$

Were A is the $(N \times 5)$ matrix of $1, I_{^{214}\text{Pb}}, I_{^{214}\text{Bi}}, I_{^{208}\text{Tl}}, I_{^{212}\text{Pb}}$ coefficients, with one row for each measurement; $\vec{x}_i$ are the unknown fundamental spectra of each component in the bin i; and $\vec{s}_i$ is the count rate that was actually measured in the channel i at each measurement.

Note that the system has to be constructed and solved for every energy bin. In our case, we have 1000 spectral channels, implying that the minimization happens 1000 times, with the same A matrix and varying $\vec{s}_i$. Although apparently cumbersome, with our Python implementation it is possible to complete the task in few seconds in a regular laptop. Key to achieve this is the SciPy (Virtanen et al., 2020) package `optimize.nnls` that follows a numerical recipe from Lawson and Hanson (1995). Aside from being very optimized, this method returns by construction positive values for the unknowns, which is the type of solution relevant, as each unknown represents a count rate in a spectrum.

Although mathematically and computationally possible, the system with five unknowns does not separate correctly the components for

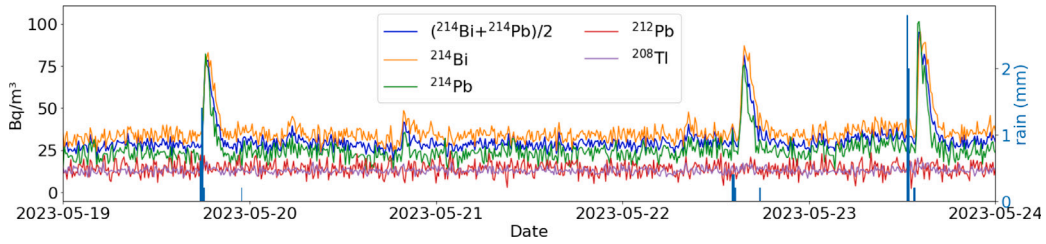

Fig. 1. Example of time series of the integrals of the photo-peaks from ^{214}Bi, ^{214}Pb, ^{212}Pb, and ^{208}Tl. This particular data set was recorded by the monitor at the town of Torre de l'Espanyol (southern Catalonia), featuring a $2'' \times 2''$ $LaBr_3$(Ce) scintillator in direct measurement configuration. The right axis displays the rain accumulated in intervals of 10 min. Note the coincidence of the rain episodes with spikes in the ^{214}Pb and ^{214}Bi activity concentration.

^{214}Pb and that for ^{214}Bi. This implies that these two components are not independent. Physically, this implies that ^{214}Pb and ^{214}Bi are in equilibrium when they are scavenged from the clouds (Patiris et al., 2023), which is quite plausible given their half-lives in the range of tens of minutes.

Having found that the variations of ^{214}Pb and ^{214}Bi are not independent, we construct a new variable x_w representing the combined fundamental spectrum of the ^{214}Pb and ^{214}Bi photo-peaks, and their resulting Compton and bremsstrahlung. We dub this x_w the *weather component*. In the system of equations x_w has a new coefficient with the combined information from ^{214}Bi and ^{214}Pb. We define $W \equiv (I_{214\text{Pb}} + I_{214\text{Bi}})/2$ for this purpose. The choice is supported from the fact that ^{214}Pb and its daughter ^{214}Bi appear to be in equilibrium when they are washed out in rain episodes (Fig. 1). Finally, we solve the system of equations with four unknowns:

$$\begin{cases} s_i^{(1)} = x_{0,i} + W^{(1)} x_{w,i} + I^{(1)}_{208\text{Tl}} x_{3,i} + I^{(1)}_{212\text{Pb}} x_{4,i} \\ \cdots \\ s_i^{(N)} = x_{0,i} + W^{(N)} x_{w,i} + I^{(N)}_{208\text{Tl}} x_{3,i} + I^{(N)}_{212\text{Pb}} x_{4,i} \end{cases} \tag{4}$$

3. Results

As a result we obtain the constant background, the weather component, and the ^{212}Pb and ^{208}Tl fundamental spectra for each of the monitors under consideration. As representative cases we show the four-component separation of a $LaBr_3$(Ce) (Fig. 2(a)) and a SrI_2(Eu) detector (Fig. 2(b)). The main difference among the two is the constant background, that in the former case contains the Lanthanum internal contamination.[2] Besides this, what we have called the weather component exhibits the ^{214}Pb 242 keV, 295 keV, and 351 keV peaks, as well as the ^{214}Bi 609 keV, 768 keV, 934 keV, 1120 keV, 1238 keV, 1378 keV, and 1764 keV peaks. Although these are clear by simple inspection, ^{214}Pb and, especially, ^{214}Bi have a large number of lower-probability peaks that contribute to this component. Moreover, we also see a substantial continuum originating by the Compton-scattered emission and the bremsstrahlung of the peaks.

The fundamental spectra of ^{212}Pb and ^{208}Tl are much simpler, and exhibit a single bright peak each, and some background continuum at the lower energies. At high energies these components appear somewhat noisy in the logarithmic scale, but in fact these are just fluctuations at the range of 10^{-4} cps which may also be present in the brighter components.

The crucial point here is that each of these separated components have a spectral shape that has been computed from the data, and that takes into account not only the photo-peaks, but also the resulting continuum. This continuum is the part that is expected to have a shape dependent on the characteristics of the monitor and of the surroundings.

[2] Internal contamination by Lanthanum generates two strong peaks at 1436 and 1468 keV, which are less separated than the energy resolution at those energies.

We also notice that the constant background contains little bumps at the locations of the main peaks of the other components. We attribute this to the presence of these isotopes even in absence of rain. The constant background component keeps the minimum height of each peak, whereas each of the isotope-specific components account for the part that varies. In Fig. 3 we compare the constant background of various $LaBr_3$(Ce) and SrI_2(Eu) detectors.

By comparing the constant background for each monitor we can appreciate how specific the Compton and bremsstrahlung components are. Monitor 9 (Roses) for instance (Fig. 3(a)) exhibits a reduced continuum at low energies owing to the fact that it is a detector with a particulate filter. In such detector the crystal is shielded from all sides except the one facing the filter, thus greatly reducing the background photons. Moreover, a pump forces air flow through the filter, hence concentrating the natural emitters. As a result, and compared to other monitors, the weather component of Roses has the highest intensity relative to the constant background.

Another clear difference appears on monitor 18 (Sant Jaume d'Enveja), which has a $1'' \times 1''$ crystal. This implies a factor 8 less sensitive volume than the $2'' \times 2''$, and hence the reduced count rate throughout the spectrum. Even in the case that the monitors have the exact same configuration, such as monitor 33 (Pratdip) and 90 (in our lab), we can visually realize the different shape of the background (especially at low energies), and the height of the ^{40}K peak. Overall the constant background is always higher in our lab, which is a closed room with concrete walls surrounding the equipment. Instead, the field monitors are usually on poles facilitating an uninterrupted field of view for the crystal.

4. Validation

Having obtained highly specific fundamental spectra from constant background and prominent natural gamma-ray emitters from various monitors permit us to showcase the versatility of our method. To show now the capability of spectral reconstruction, we analyze spectra that were recorded subsequently, and that were not used to generate the fundamental spectra. For this, let us now focus on the monitor 31 (Torre de l'Espanyol) which is one of the most modern among the very extended type of monitors with $LaBr_3$(Ce) crystals. The analysis with any other monitor of the network would be equivalent.

On June 11th 2023 at Torre de l'Espanyol had not rained for more than two weeks. That day at about 17:00 local time it started to rain. At about 18:40 the activity concentration of ^{222}Rn descendants peaked at a value about three times higher than the average from the previous days of stable weather. As a first exercise, we use the fundamental spectra from Fig. 2(a) to reconstruct the first spectrum of June 11th (Fig. 4(a)), with low activity concentration of natural emitters; and the spectrum from that day at 18:40, with high activity concentration of natural emitters (Fig. 4(b)).

As it can be seen in Fig. 4, the fundamental spectra generated from May 2023 data are capable of perfectly reconstructing spectra from June 11th 2023. As usual in Lanthanum detectors, the spectra are largely dominated by the constant background. In the first spectrum

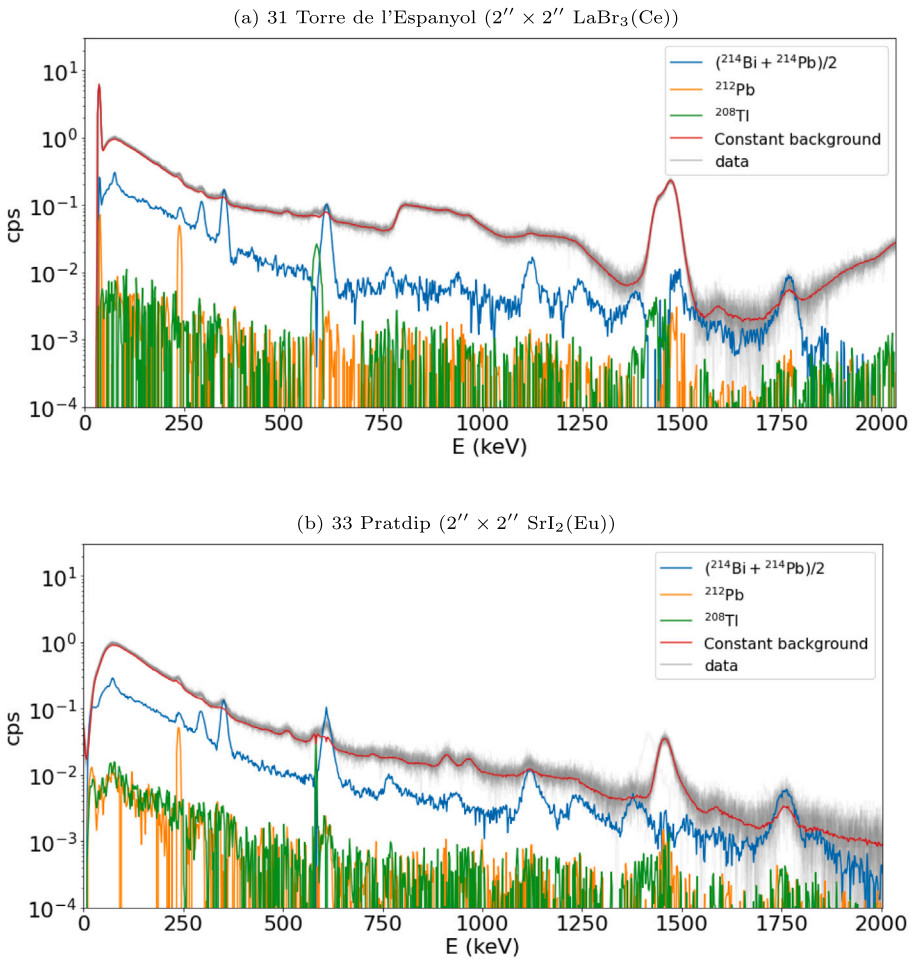

Fig. 2. Spectra of the ^{214}Bi+^{214}Pb, ^{212}Pb, ^{208}Tl, and constant background components for monitor 31 (top) and 33 (bottom). On top of the separated components we have included one spectrum per day of the May 2023 dataset, showcasing the variability in the repetitive measurements.

of the day the ^{214}Pb and ^{214}Bi peaks barely stand out from their base value. Later, the weather component varied by a large margin, not only making more prominent the photo-peaks, but also the continuum at all energies below the highest energy peaks of the ^{214}Bi. Also in Fig. 4 we added the residuals of the fit to the data by the combination of fundamental spectra. We do the residual plot in units of the expected model count rate, and taking into account the Poisson uncertainty of the counts in each spectral channel. This way we can immediately see that the residuals are compatible with zero at all energies.

Next we apply the procedure described above to all the spectra from June 11th 2023. The coefficients of each fit are the activity concentrations, so we can produce time series of the fit coefficients (Fig. 5). We also compare the values that we get to established methods, like Gaussian fitting, and the proportional ROI cleaning method (Cerezo et al., 2023). We focus on the combined activity of ^{214}Pb and ^{214}Bi, that we dubbed the weather component, because is the one that strongly varies during the day. The three time series show compatible values of activity concentration of all three methods.

5. Conclusions

We started this analysis with the assumption that all of the gamma-emitting Radon descendants that we have considered would be variable with weather, and that the strong variations would provide the lever arm to solve Eq. (4). As it turned out, in our measurements only ^{222}Rn descendants are weather dependent. Patiris et al. (2023) provided a comprehensive explanation of how both ^{220}Rn and ^{222}Rn do end up in clouds, but only ^{222}Rn descendants are washed out in case of rain. This is due to the fact that the time scale of the cloud formation and rain is much longer than the ^{220}Rn half-life of ~ 55 s. This is certainly confirmed in our data sets, and has two interesting implications. On one hand, the fundamental spectra of ^{214}Bi and ^{214}Pb become inseparable because strong variations occur simultaneously in case of rain. On the other hand, we find that it is not necessary to have strong variations of the isotopes for which we can monitor the intensity in order to separate the spectra.

The latter conclusion implies that our method is capable of locking on the variations induced by the Poisson fluctuations rather than by varying concentration of the isotope. In fact, other than Radon descendants we can draw our attention to ^{40}K, which is fixed to the soil and the construction materials surrounding the detector, but its concentration does not vary. By adding an extra unknown in Eq. (4) and performing the same exercise as for the Radon descendants, we can find the fundamental spectrum of ^{40}K in case of monitors that do not contain Lanthanum, whose internal contamination coincides with the ^{40}K 1461 keV photo-peak. Reminiscent of what happens with the minimum quantity of Radon descendants, the ^{40}K component is somewhat confused with the constant background (Fig. 6), but the location of the photo-peak is correctly estimated, and the resulting Compton scattering is accounted for. When used as a template, this spectrum could be scaled up to fit a new measurement. Therefore we postulate that it is possible to obtain fundamental spectra for any photo-peak for which we can obtain a coefficient proportional to its intensity in every measurement.

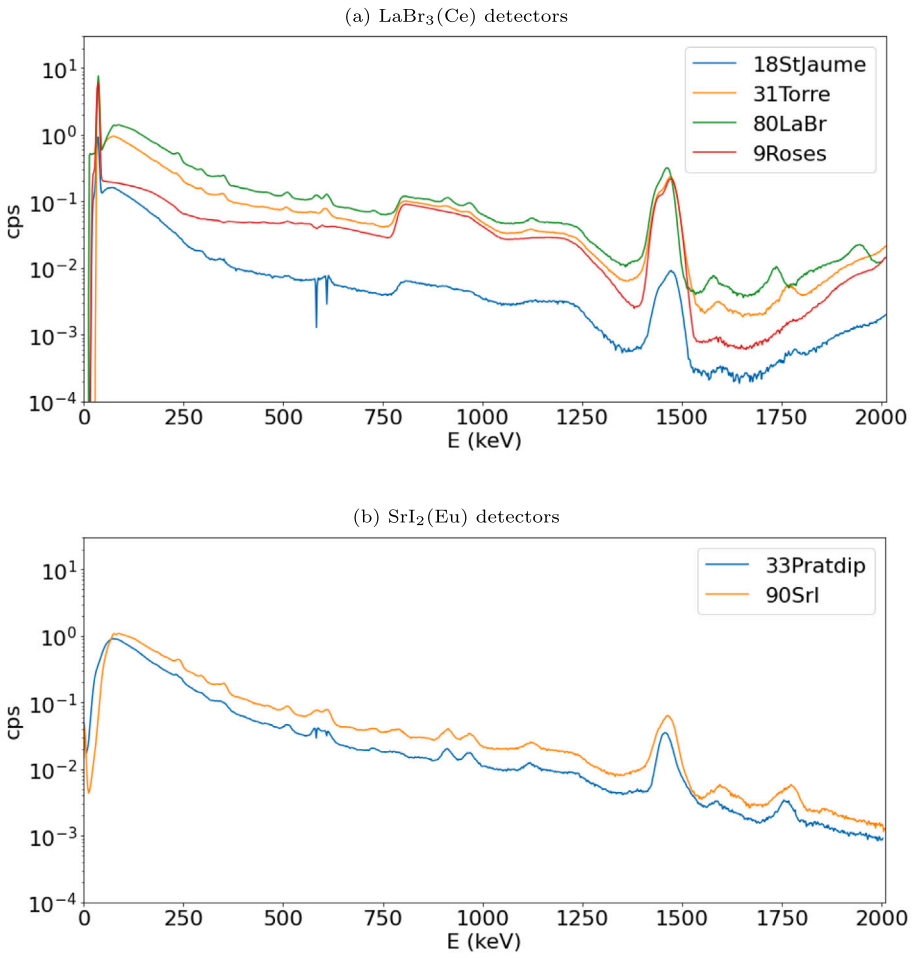

Fig. 3. Spectra of the constant background component from the four $LaBr_3(Ce)$ detectors (top) and the two $SrI_2(Eu)$ detectors (bottom) under study.

Our method is suitable for the generation of fundamental spectra from repetitive measurements, regardless of the amplitude of the intensity variations of the isotopes of interest. It is important though to have a large number of measurements. When the experimental setup is not as favorable as ours, this translates into splitting the total measurement time into many short-duration spectra (that can be later combined anyway). The main difficulty in this case will be to have good estimates for the intensity of each photo-peak of each individual spectrum. This is particularly true for overlapping peaks in detectors with limited energy resolution where, e.g., the ^{212}Pb (238.6 keV) and the ^{214}Pb (242.0 keV) peaks may be hard to disentangle.

Having extracted a set of detector-specific spectral components allows for an extremely detailed spectral reconstruction upon recording a new measurement. Once the $\vec{x}_i$ in Eq. (4) are no longer unknown, the activity concentrations can be measured by component fitting (FSA). In practice, this implies to find the activity concentrations W, $I_{208\mathrm{Tl}}$, $I_{212\mathrm{Pb}}$, which is the inverse problem to the one that we solve here. The reconstruction procedure fits the whole spectrum rather than a number spectral windows, which makes it less fluctuating than the Gaussian fitting, and requires less fit parameters. Also, we have found that we obtain results compatible to those from the ROIs method, which is currently the standard procedure of our monitoring system.

Finding the fundamental spectra is an operation that requires some tens of megabytes of spectral data, but once the data are retrieved, the minimization procedure is performed in a matter of seconds in a regular laptop. Nevertheless this operation has to be performed only once per detector, or until there is a significant change in its components or surroundings. The next step, using the fundamental spectra to reconstruct any new spectrum, takes negligible computer power and is easily scalable to operate in the whole network.

With the recorded fundamental spectra, in the event that an artificial isotope shows up, it will be easy to pinpoint as a spectral feature not comprised in the recurrent components, and evident in the residuals plot (Fig. 4). In an upcoming publication we will propose a method to systematically search for anomalies in the spectral reconstruction from fundamental spectra, while also dealing with the low-counts issue mentioned above.

CRediT authorship contribution statement

Ignasi Reichardt: Writing – review & editing, Writing – original draft, Visualization, Software, Methodology, Investigation, Formal analysis. **Agustín Cerezo:** Writing – review & editing, Data curation. **Elena Prieto:** Writing – review & editing, Project administration. **Marçal Salvadó:** Writing – review & editing, Supervision, Resources, Project administration, Funding acquisition, Conceptualization.

Declaration of competing interest

The authors declare that they have no known competing financial interests or personal relationships that could have appeared to influence the work reported in this paper.

Data availability

Data will be made available on request.

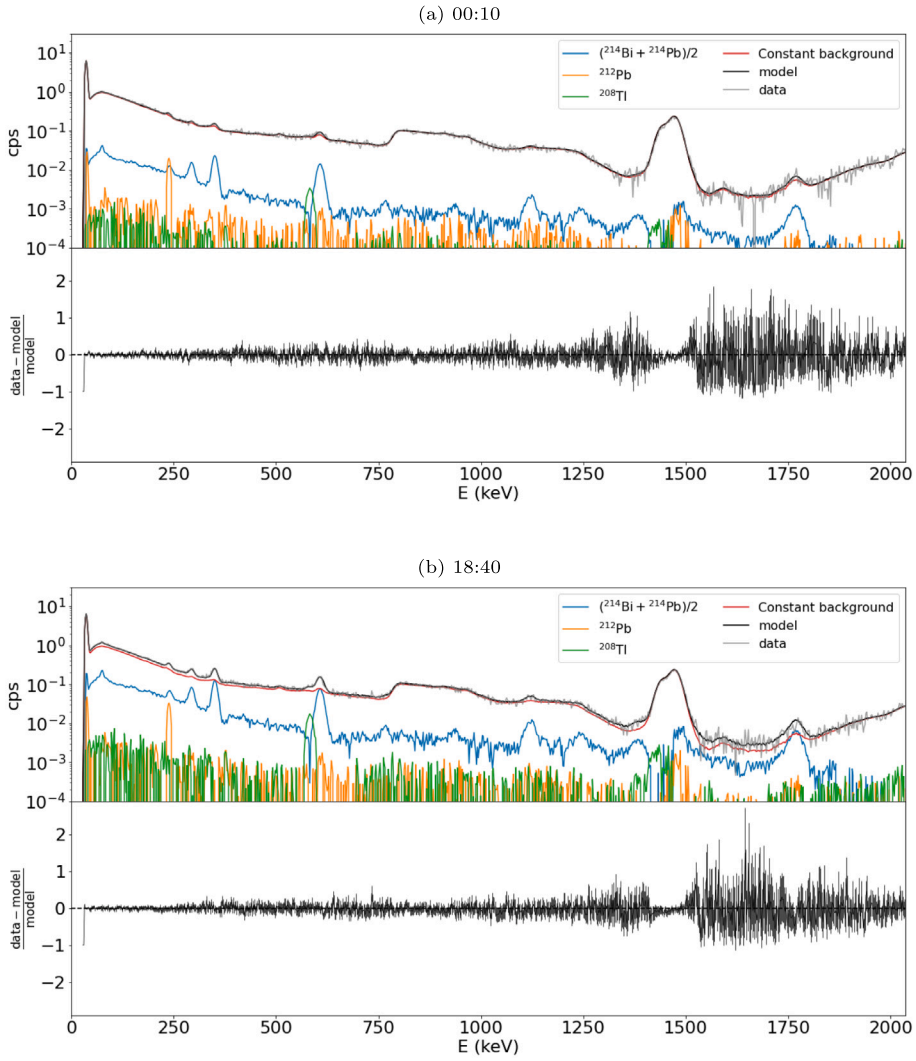

Fig. 4. Spectra recorded at monitor 31 (Torre de l'Espanyol) on June 11th 2023 at 00:10 (top) and 18:40 (bottom). The noisy, shaded gray curve is the actual measurement. The black curve is the model resulting from the linear combination of fundamental spectra from Fig. 2(a). Below the spectra we show the error bars of the residuals of the fit.

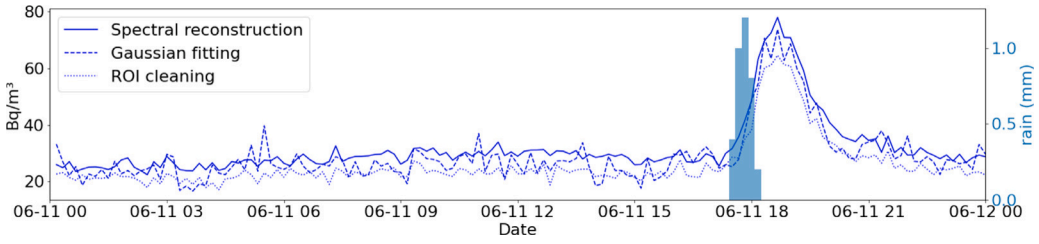

Fig. 5. Time series of the weather component at monitor 31 (Torre de l'Espanyol) on June 11th 2023. The same quantity is computed using three methods: the spectral reconstruction from this work (solid line); Gaussian fitting (dashed line); and the proportional ROI cleaning method from Cerezo et al. (2023). The x axis labels are month-day hour of the day (local). The right axis displays the rain accumulated in intervals of 10 min.

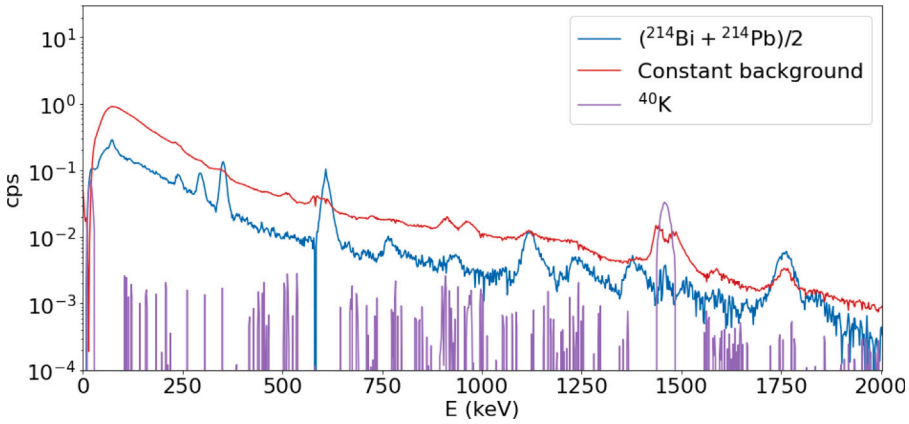

Fig. 6. Separation of the constant background, the weather component, and the ^{40}K component for the monitor 90 (see Table 1). ^{212}Pb and ^{208}Tl are also included in the system of equations, but not shown for simplicity.

References

Abida, R., Bocquet, M., Vercauteren, N., Isnard, O., 2008. Design of a monitoring network over France in case of a radiological accidental release. Atmos. Environ. 42 (21), 5205–5219. http://dx.doi.org/10.1016/j.atmosenv.2008.02.065, URL: https://www.sciencedirect.com/science/article/pii/S1352231008002409.

Androulakaki, E., Kokkoris, M., Tsabaris, C., Eleftheriou, G., Patiris, D., Pappa, F., Vlastou, R., 2016. In situ γ-ray spectrometry in the marine environment using full spectrum analysis for natural radionuclides. Appl. Radiat. Isot. 114, 76–86. http://dx.doi.org/10.1016/j.apradiso.2016.05.008, URL: https://www.sciencedirect.com/science/article/pii/S0969804316301798.

Ángeles Ontalba, M., Ángel Corbacho, J., Baeza, A., Vasco, J., Caballero, J.M., Valencia, D., Baeza, J.A., 2022. Radiological Alert Network of Extremadura (RAREx) at 2021:30 years of development and current performance of real-time monitoring. Nucl. Eng. Technol. 54 (2), 770–780. http://dx.doi.org/10.1016/j.net.2021.08.007, URL: https://www.sciencedirect.com/science/article/pii/S1738573321004939.

Baeza, A., Corbacho, J., Caballero, J., Ontalba, M., Vasco, J., Valencia, D., 2017. Development of an advanced radioactive airborne particle monitoring system for use in early warning networks. J. Radiol. Prot. 37 (3), 642.

Caciolli, A., Baldoncini, M., Bezzon, G., Broggini, C., Buso, G., Callegari, I., Colonna, T., Fiorentini, G., Guastaldi, E., Mantovani, F., et al., 2012. A new FSA approach for in situ γ ray spectroscopy. Sci. Total Environ. 414, 639–645.

Casanovas, R., Morant, J., Salvadó, M., 2012a. Energy and resolution calibration of NaI(Tl) and LaBr3(Ce) scintillators and validation of an EGS5 Monte Carlo user code for efficiency calculations. Nucl. Instrum. Methods Phys. Res. A 675, 78–83. http://dx.doi.org/10.1016/j.nima.2012.02.006, URL: https://www.sciencedirect.com/science/article/pii/S0168900212001490.

Casanovas, R., Morant, J., Salvadó, M., 2012b. Temperature peak-shift correction methods for NaI(Tl) and LaBr3(Ce) gamma-ray spectrum stabilisation. Radiat. Meas. 47 (8), 588–595. http://dx.doi.org/10.1016/j.radmeas.2012.06.001, URL: https://www.sciencedirect.com/science/article/pii/S1350448712001692.

Casanovas, R., Morant, J.J., Salvadó, M., 2014. Development and calibration of a real-time airborne radioactivity monitor using gamma-ray spectrometry on a particulate filter. IEEE Trans. Nucl. Sci. 61 (2), 727–731. http://dx.doi.org/10.1109/TNS.2014.2299715.

Casanovas, R., Prieto, E., Salvadó, M., 2016. Calculation of the ambient dose equivalent H*(10) from gamma-ray spectra obtained with scintillation detectors. Appl. Radiat. Isot. 118, 154–159.

Cerezo, A., Prieto, E., Reichardt, I., Casanovas, R., Salvadó, M., 2023. A fast algorithm for real-time monitoring of artificial radioisotopes in presence of variable natural radioactivity. Radiat. Phys. Chem. 209, 110946. http://dx.doi.org/10.1016/j.radphyschem.2023.110946, URL: https://www.sciencedirect.com/science/article/pii/S0969806X23001913.

Cerezo, A., Reichardt, I., Prieto, E., Casanovas, R., Rovira, C., Salvadó, M., 2024. Comprehensive remote calibration of detectors in a radiological surveillance network: From basic response to high-level data analysis. Radiat. Phys. Chem. submitted for publication.

CSN, 2023. Instrucción IS-10, revisión 2, de 7 de septiembre de 2023, del Consejo de Seguridad Nuclear, por la que se establecen los criterios de notificación de sucesos al Consejo por parte de las centrales nucleares. https://www.boe.es/eli/es/ins/2023/09/07/is10.

Fujinami, N., 1996. Observational study of the scavenging of radon daughters by precipitation from the atmosphere. Environ. Int. 22, 181–185. http://dx.doi.org/10.1016/S0160-4120(96)00106-7, URL: https://www.sciencedirect.com/science/article/pii/S0160412096001067. The Natural Radiation Environment VI.

Hiemstra, P.H., Pebesma, E.J., Twenhöfel, C.J., Heuvelink, G.B., 2009. Real-time automatic interpolation of ambient gamma dose rates from the Dutch radioactivity monitoring network. Comput. Geosci. 35 (8), 1711–1721. http://dx.doi.org/10.1016/j.cageo.2008.10.011, URL: https://www.sciencedirect.com/science/article/pii/S0098300409000867.

Lawson, C.L., Hanson, R.J., 1995. Solving Least Squares Problems. Society for Industrial and Applied Mathematics.

Neumaier, S., Dombrowski, H., Kessler, P., 2016. Metrology for radiological early warning networks in Europe ("METROERM")—A joint European metrology research project. Health Phys. 111 (2), 100–105.

Paatero, J., Hatakka, J., 1999. Wet deposition efficiency of short-lived radon-222 progeny in central Finland. Boreal Environ. Res. 4 (4), 285–294, URL: https://www.borenv.net/BER/archive/pdfs/ber4/ber4-285-293.pdf.

Patiris, D., Tsabaris, C., Livanou, K., Roumelioti, S.K., Alexakis, S., 2023. Atmospheric in situ gamma-ray spectrometry for precipitation investigation. Acta Geophys. 1–17. http://dx.doi.org/10.1007/s11600-023-01090-9.

Stöhlker, U., Bleher, M., Doll, H., Dombrowski, H., Harms, W., Hellmann, I., Luff, R., Prommer, B., Seifert, S., Weiler, F., 2018. The German dose rate monitoring network and implemented data harmonization techniques. Radiat. Prot. Dosim. 183 (4), 405–417. http://dx.doi.org/10.1093/rpd/ncy154, arXiv:https://academic.oup.com/rpd/article-pdf/183/4/405/28882512/ncy154.pdf.

Toivonen, H., Vesterbacka, K., Pelikan, A., 2008. LaBr 3 spectrometry for environmental monitoring. URL: https://inis.iaea.org/search/43003958.

USNRC, 2021. Appendix B to part 20—Annual Limits on Intake (ALIs) and Derived Air Concentrations (DACs) of radionuclides for occupational exposure; effluent concentrations; concentrations for release to sewerage. https://www.nrc.gov/reading-rm/doc-collections/cfr/part020/part020-appb.html.

Virtanen, P., Gommers, R., Oliphant, T.E., Haberland, M., Reddy, T., Cournapeau, D., Burovski, E., Peterson, P., Weckesser, W., Bright, J., van der Walt, S.J., Brett, M., Wilson, J., Millman, K.J., Mayorov, N., Nelson, A.R.J., Jones, E., Kern, R., Larson, E., Carey, C.J., Polat, İ., Feng, Y., Moore, E.W., VanderPlas, J., Laxalde, D., Perktold, J., Cimrman, R., Henriksen, I., Quintero, E.A., Harris, C.R., Archibald, A.M., Ribeiro, A.H., Pedregosa, F., van Mulbregt, P., SciPy 1.0 Contributors, 2020. SciPy 1.0: Fundamental algorithms for scientific computing in Python. Nature Methods 17, 261–272. http://dx.doi.org/10.1038/s41592-019-0686-2.